Dielectric properties of twist grain boundary phases: Influence of the anchoring and the distance between grain boundaries

M. Ismaïli,* F. Bougrioua, and N. Isaert
Laboratoire de Dynamique et Structure des Matériaux Moléculaires, ESA CNRS 8024, Université de Lille 1, F-59655 Villeneuve d'Ascq Cedex, France

C. Legrand
Département Hyperfréquences et Semiconducteurs, Institut d'Electronique et de Microélectronique du Nord, UMR 9929, Université de Lille 1, F-59655 Villeneuve d'Ascq Cedex, France
and Laboratoire d'Etudes des Matériaux et Composants pour l'Electronique, Université du Littoral, Maison de la Recherche Blaise Pascal - BP 717, F-62228 Calais Cedex, France

H. T. Nguyen
Centre de Recherche Paul Pascal, Université de Bordeaux 1, Avenue A. Schweitzer, F-33600 Pessac, France
(Received 21 March 2001; published 7 December 2001)

The dielectric properties of the twist grain boundaries TGB_A and TGB_C of liquid crystal phases differ from the smectic-*A* and smectic-*C** phase ones: a theoretical model confirmed by experimental results shows that the Goldstone mode of the TGB_C phase and the soft mode of the TGB_A phase are strongly reduced. This behavior is due to elastic strain, which is connected to two parameters: the anchoring at the grain boundaries and the distance between the grain boundaries. It is shown quantitatively that a relatively flexible anchoring in the TGB_A phase becomes rigid in the TGB_C one. The relaxation frequencies of these modes allow analysis of the rotational viscosity variations.

DOI: 10.1103/PhysRevE.65.011701 PACS number(s): 61.30.Eb, 51.70.+f, 77.84.−s

I. INTRODUCTION

In 1988, Renn and Lubensky proposed a theoretical structure of the twist grain boundary (TGB) phases [1]. Since the synthesis of the TGB_A phase by Goodby *et al.* in 1989 [2] and the TGB_C phase by Nguyen *et al.* [3] in 1992, several studies have been devoted to these phases [4–8]. The TGB_A and TGB_C structures have been established from optical and x-ray studies [5,6]: the TGB_A and TGB_C phases are twisted structures, made up by blocks of smectic-*A* (Sm-*A*) and Sm-*C*. Optical studies of the helical pitch [4,7] show that the helical pitch varies from approximately a micrometer to a fraction of a micrometer and bears variations that are typical of phases and phase sequences. X-ray studies [5,6,8] show that the helical axis is parallel to the smectic layers in TGB_A and is tilted in the TGB_C phase with an angle close to smectic-*C* tilt angle; these studies also led to the determination of the number of TGB blocks per pitch.

The first studies of dielectric properties show that in the TGB_A [9–13] and TGB_C [13] phases, like in the Sm-*A* and Sm-*C** phases, the electric field induces amplitude fluctuations of the tilt angle (soft mode [14,15]) and phase fluctuations of the tilt angle (Goldstone mode [14,15]). Wróbel *et al.* [11] show that in the TGB_A phase, the soft mode relaxation process behavior differs from that anticipated by the extended mean-field theory. Xu *et al.* [12] show also the existence of the soft mode in the TGB_A phase and highlight the existence of a low frequency mode assigned to the relaxation process in the grain boundaries. Our preliminary studies of dielectric properties of the TGB_A and TGB_C phases [13] confirm the existence of the soft mode in the TGB_A phase and show the existence of a Golstone mode in the TGB_C phase. We highlighted the dielectric behavior difference between TGB_A and TGB_C phases and put into evidence the influence of the block structure: the TGB phase relaxation processes have lower amplitudes and higher frequencies in comparison with those of classical Sm-*A* and Sm-*C* phases.

In this paper, we report a detailed study of the dielectric properties of the TGB_A and TGB_C phases when the electric field is parallel to the helical axis. A theoretical model is given in the first part. It leads to the expressions of the dielectric amplitudes $\Delta\epsilon$ and relaxation frequencies f_c of the two modes. New elastic parameters are introduced and justified, depending on the size of the TGB blocks and on the strength of the anchoring at the grain boundaries. The second part concerns experimental studies of the first chemical series with the TGB_C phase synthesized by Nguyen *et al.* [3] and characterized by a rich polymorphism. Experimental results obtained in several compounds bearing Sm-*C**, Sm-*A*, TGB_C, TGB_A, and N* phases are reported and analyzed; the block structure and the block size clearly influences the dielectric properties of the TGB phases. The anchoring strength at the grain boundaries, and its variations according to temperature are deduced from experimental results. The rotational viscosities close to the Sm-*C**-TGB_A and Sm-*C**–TGB_C phases transitions are analyzed.

II. THEORY

A. TGB structure

In the following, we will only consider one block of the TGB structure; other blocks have the same features. Figure 1

*Author to whom correspondence should be addressed. Electronic address: Mimoun.Ismaili@univ-lille1.fr

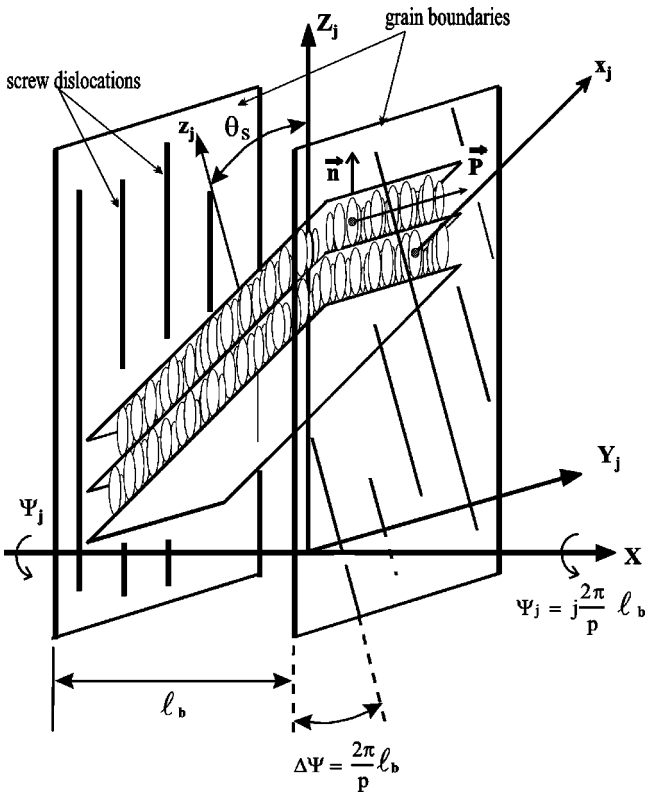

FIG. 1. Block structure of the TGB_C phase.

shows the structure of the jth block, which is turned by an angle $\Psi_j = j(2\pi/p)l_b$ around the helical axis with respect to a reference block ($j=0$); p represents the helical pitch and l_b the block width. Two reference systems, (OXY_jZ_j) and $(Ox_jY_jz_j)$, are used to describe the TGB structure. The first one is connected with the grain boundary (Y_jZ_j) planes and the helical axis OX. The second one is connected with the smectic layer (x_jY_j) planes and the layer normal (Oz_j). According to Navailles *et al.* [5,6], the TGB_C structure is helielectric; the spontaneous polarization P_S lies along OY_j, and the first reference system (OXY_jZ_j) is rotated by an angle θ_S around the OY_j axis with respect to the second one $(Ox_jY_jz_j)$, θ_S being the spontaneous tilt angle. For the TGB_A phase $\theta_S=0$ and the two systems coincide.

The director components in the layers system is given by

$$n_{x_j} = \sin\theta\cos\varphi,$$

$$n_{Y_j} = \sin\theta\sin\varphi, \tag{1}$$

$$n_{z_j} = \cos\theta.$$

θ and φ are, respectively, the well known director tilting and azimuthal angles.

The director components along OX and OZ_j directions, n_X and n_{Zj}, are linear combinations of n_{xj} and n_{zj} in OXY_jZ_j,

$$n_X = \cos\theta_s n_{x_j} - \sin\theta_s n_{z_j},$$

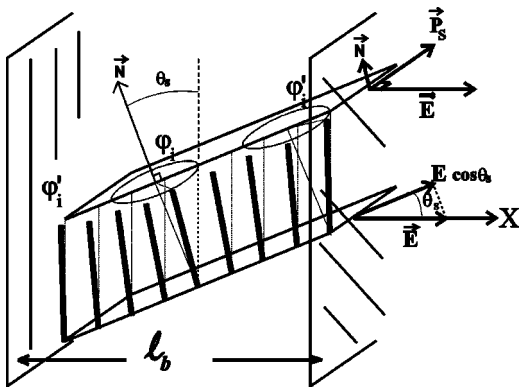

FIG. 2. Molecular rotation around the cone induced by the electric field in the TGB_C phase.

$$n_{Z_j} = \sin\theta_s n_{x_j} + \cos\theta_s n_{z_j}. \tag{2}$$

At zero field, $\theta=0$ and φ is indefinite in TGB_A, $\theta=\theta_S$ and $\varphi=0$ in TGB_C. Nonzero field induces director tilt and azimuthal angle changes, but is not supposed to induce any tilt or rotation of the layers.

B. Free-energy density

Let us introduce the free-energy density of the TGB phases, when an electric field is applied,

$$g = g_0 + E_{elast} - \vec{P}\cdot\vec{E}.$$

g_0 is a simple Landau expansion describing the smectic-A–smectic-C transition,

$$g_0 = \frac{1}{2}a\theta^2 + \frac{1}{4}b\theta^4 + \frac{1}{2\epsilon_0\chi}(P_X^2 + P_{Y_j}^2 + P_{Z_j}^2) - C(P_{Y_j}\theta\cos\varphi - P_{x_j}\theta\sin\varphi), \tag{3}$$

where a is supposed to be temperature dependent: $a=\alpha(T-T_0)$, T_0 representing the Sm-A–Sm-C transition temperature in the case of a nonchiral compound, b is positive, and C expresses the linear coupling between the tilt and the polarization. In particular, Eq. (3) leads to the expressions of the spontaneous polarization and tilt of the Sm-C phase: $P_s = \epsilon_0\chi C\theta_s$, $\theta_s = \sqrt{\alpha(T_C-T)/b}$ with $T_C = T_0 + \epsilon_0\chi C^2/\alpha$. The polarization component P_{x_j} can be developed as

$$P_{x_j} = P_X\cos\theta_s + P_{Z_j}\sin\theta_s.$$

E_{elast} is the elastic distortion energy of the nematic director in the smectic layers; we will indeed see that the director's components in a given block submitted to an electric field are not constant: a twist deformation is expected when the field is perpendicular to the helical axis, but other orientations can also give rise to splay distortions [13].

C. Director rotations induced by an electric field parallel to the helical axis in the TGB phases

Figures 2 and 3 schematically describe the azimuthal angle φ and tilt angle θ induced in TGB_C and TGB_A phases

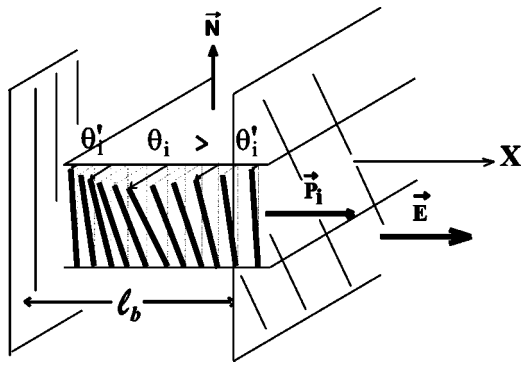

FIG. 3. Tilt angle induced by electric field in the TGB_A phase; distortion due of the anchorage at the grain boundaries.

submitted to an electric field parallel to the helical axis. In the TGB_C phase, the field component along the smectic layers $E_{x_j}=E_X\cos\theta_S$ is perpendicular to the spontaneous polarization $\vec{P}_S=\epsilon_0\chi C\theta_S\ \vec{u}_{Y_j}$, where $\vec{u}_{Y_j}$ is a unit vector parallel to OY_j. Figure 2 schematically shows that, in the smectic layers, induced molecular rotations around the cone are expected because of the torque exerted by the field on the polarization. They correspond to the so-called Goldstone mode.

In a given block, the rotation is not uniform: if the grain boundary exerts some anchorage on the director, we can reasonably assume that it is larger in the center of the block and weaker near the grain boundary. There appears then, a sort of twist deformation of the director, this deformation induces an elastic torque.

Figure 3 schematically shows that we can expect a soft mode in the TGB_A phase connected to a field induced polarization $\vec{P}_i$. The whole $\vec{E}_X$ field is efficient to create it as, in the TGB_A phase, $\theta_S=0$ and so $\vec{E}_{x_j}=\vec{E}_X$. If the induced tilting is not uniform, there appears again a twist deformation of the director.

We finally remark that in such a description, the induced rotation $\theta(X)$ in the TGB_A and $\theta_s\varphi(X)$ in the TGB_C are in fact mean values of two variable functions $\theta(X,Y_j)$ and $\theta_s\varphi(X,Y_j)$ which are Y_j averaged over the distance between two screw dislocations. We also note that these effects are j independent: all blocks are subject to the same phenomena.

D. The Goldstone mode of the TGB_C phase

For the TGB_C phase, the free energy can locally be written as

$$g=\frac{1}{2}\alpha(T-T_0)\theta_S^2+\frac{1}{4}b\theta_S^4+\frac{1}{2\epsilon_0\chi}(P_X^2+P_Y^2+P_Z^2)-C[P_{Y_j}\theta_S\cos\varphi-(P_X\cos\theta_S+P_{Z_j}\sin\theta_S)\theta_S\sin\varphi]+\frac{1}{2}K_{22}\theta_S^2\left(\frac{d\varphi}{dX}\right)^2-P_XE_X. \tag{4}$$

The term $\frac{1}{2}K_{22}\theta_S^2(d\varphi/dX)^2$ is the energy density associated to the twist deformation. Minimization of Eq. (4) with respect to P_{Z_j}, P_{Y_j}, P_X, and φ gives

$$P_{Z_j}=-\epsilon_0\chi C\theta_S\sin\theta_S\sin\varphi, \tag{5}$$

$$P_{Y_j}=\epsilon_0\chi C\theta_S\cos\varphi, \tag{6}$$

$$P_X=\epsilon_0\chi E_X-\epsilon_0\chi C\theta_S\cos\theta_S\sin\varphi, \tag{7}$$

$$C[P_{Y_j}\sin\varphi+(P_X\cos\theta_S+P_{Z_j}\sin\theta_S)\cos\varphi]-K_{22}\theta_S\left(\frac{d^2\varphi}{dX^2}\right)=0. \tag{8}$$

Replacing P_X, P_{Y_j}, and P_{Z_j} in Eq. (8) leads to

$$\theta_S\frac{d^2\varphi}{dX^2}\simeq\frac{\epsilon_0\chi CE_X\cos\theta_S}{K_{22}}, \tag{9}$$

then

$$\theta_S\frac{d\varphi}{dX}=\frac{\epsilon_0\chi CE_X\cos\theta_S}{K_{22}}X, \tag{10}$$

the solution is a parabolic deformation,

$$\theta_S\varphi=\frac{\epsilon_0\chi CE_X\cos\theta_S}{2K_{22}}\left[X^2-\left(\frac{l_b}{2\beta}\right)^2\right]. \tag{11}$$

In this expression, the coefficient $0\leqslant\beta\leqslant1$ describes the molecular anchoring at the grain boundaries: if the anchoring is rigid, $\beta=1$ and $\varphi=0$ for $X=\pm l_b/2$; if the anchoring is not rigid ($\beta\neq1$), $\varphi=0$ for a fictive distance $X_0=l_b/2\beta$, which is larger than $l_b/2$.

The mean rotation can then be calculated for $-l_b/2<X<l_b/2$ and the mean polarization $\langle P_X\rangle$ along the applied field ($\langle P_X\rangle$ is j independent and P_{Y_j} and P_{Z_j} disappear after averaging on a pitch period),

$$\langle\theta_S\varphi\rangle=\epsilon_0\chi CE_X\cos\theta_S l_b^2\frac{1}{8K_{22}}\left(\frac{1}{3}-\frac{1}{\beta^2}\right),$$

$$\langle P_X\rangle=\epsilon_0\chi E_X+\frac{(\epsilon_0\chi C\cos\theta_S)^2}{\dfrac{8\beta^2}{1-\beta^2/3}\dfrac{K_{22}}{l_b^2}}E_X=\epsilon_0\chi E_X+\epsilon_0\Delta\epsilon_G E_X. \tag{12}$$

The dielectric strength of the Goldstone mode is then (see $\langle P_X\rangle$)

$$\Delta\epsilon_G=\frac{\epsilon_0\chi^2C^2}{\dfrac{8\beta^2}{1-\beta^2/3}K_{22}/l_b^2}\cos\theta_S^2=\frac{\epsilon_0\chi^2C^2}{H_2}\cos\theta_S^2 \tag{13}$$

in which we call H_2 the elastic parameter that forms the denominator,

$$H_2=\frac{8\beta^2}{1-\beta^2/3}\frac{K_{22}}{l_b^2}. \tag{14}$$

We can note that $\cos^2\theta_s$ is the result of two projections: projection of the applied field E_X on the smectic planes and projection on the X direction of the dipoles induced in the smectic planes. This geometric factor is almost equal to unity since the tilt value is rarely higher than 15° in the TGB_C phase [22]. We conclude that the Goldstone mode amplitude is attenuated by the elastic parameter H_2. This parameter plays for the TGB_C phase a similar role as $K_{33}\ q^2$ in a classical Sm-C^* chiral phase with a pitch wave vector $q = 2\pi/p$.

The elastic term H_2 that limits the Goldstone mode in the TGB_C phase is so interpreted as a consequence of anchoring effects at the grain boundaries inducing twist deformations of the director.

E. The soft mode in the TGB_A phase

The problem can be solved in a similar way for the TGB_A phase. The local free energy density is written as

$$g \simeq \frac{1}{2}\alpha(T-T_0)\theta^2 + \frac{P_X^2}{2\epsilon_0\chi} - CP_X\theta + \frac{1}{2}K_{22}\left(\frac{d\theta}{dX}\right)^2 - P_X E_X . \tag{15}$$

Minimization of Eq. (15) gives

$$P_X = \epsilon_0\chi E_X + \epsilon_0\chi C\theta,$$

$$\alpha(T-T_C)\theta - K_{22}\frac{d^2\theta}{dX^2} - \epsilon_0\chi C E_X = 0. \tag{16}$$

The solution, more complicated than for the TGB_C phase, is

$$\theta = \frac{\epsilon_0\chi C E_X}{\alpha(T-T_C)}\left(1 - \frac{e^{X/a}+e^{-X/a}}{e^{l_b/2\beta a}+e^{-l_b/2\beta a}}\right). \tag{17}$$

In this formula, a is a characteristic length, $a = \sqrt{K_{22}/\alpha(T-T_C)}$; β has the same significance as above; $\theta = 0$ for a fictive distance $X_0 = l_b/2\beta$ which is larger than $l_b/2$ if the anchoring is not rigid ($\beta < 1$). If we assume a hard anchoring, the theoretical director profile is quite similar to the one obtained by Beldon and Elston [16] who studied hard anchoring surface effects in Sm-A phases.

The average values can then be calculated for $-l_b/2 < X < l_b/2$,

$$\langle\theta\rangle = \frac{\epsilon_0\chi C E_X}{\alpha(T-T_C)}\left(1 - \frac{2a}{l_b}\frac{e^{l_b/2a}-e^{-l_b/2a}}{e^{l_b/2\beta a}+e^{-l_b/2\beta a}}\right),$$

$$\langle P_X\rangle = \epsilon_0\chi E_X + \frac{\epsilon_0^2\chi^2 C^2}{\alpha(T-T_C)}\left(1 - \frac{2a}{l_b}\frac{e^{l_b/2a}-e^{-l_b/2a}}{e^{l_b/2\beta a}+e^{-l_b/2\beta a}}\right)E_X . \tag{18}$$

This last formula does not give a convenient expression of the dielectric strength connected to the soft mode (second term of $\langle P_X\rangle$), so we prefer the following approximate expression:

$$\Delta\epsilon_s \approx \frac{\epsilon_0\chi^2 C^2}{\alpha(T-T_C) + \dfrac{8\beta^2}{1-\beta^2/3}K_{22}/l_b^2} = \frac{\epsilon_0\chi^2 C^2}{\alpha(T-T_C)+H_2} \tag{19}$$

with again,

$$H_2 = \frac{8\beta^2}{1-\beta^2/3}\frac{K_{22}}{l_b^2}. \tag{20}$$

In the TGB_A phase, the soft mode is limited by thermic and elastic effects; the elastic strain is due to anchoring effects at the grain boundaries inducing twist deformations of the director. We conclude that the soft mode of the TGB_A phase is not only limited by the $\alpha(T-T_C)$ thermic parameter like in classical A phases, but also by the H_2 elastic one.

F. Dynamic properties

A sinusoidal time dependent field with frequency f is now applied to the system,

$$\vec{E}_X(t) = \vec{E}_X e^{j2\pi ft}.$$

The equations have then to include the rotational viscosities γ'_G for the Goldstone mode of the TGB_C phase, γ_s for the soft mode of the TGB_A phase. For the TGB_C phase, the torque equation (8) [including Eqs. (5)–(7)] becomes

$$\epsilon_0\chi C E_X\cos\theta_s - K_{22}\theta_S\frac{d^2\varphi}{dX^2} \simeq -j\,2\pi f\,\gamma'_G\theta_s\varphi \tag{21}$$

and for the TGB_A phase, the torque equation (16) becomes

$$-\epsilon_0\chi C E_X + \alpha(T-T_C)\theta - K_{22}\frac{d^2\theta}{dX^2} = -j2\pi f\,\gamma_s\theta. \tag{22}$$

The resolution of these equations leads to the mean values of the induced polarizations connected to the Goldstone and soft modes. In the TGB_C phase

$$\langle P_{X_G}\rangle = \frac{\epsilon_0^2\chi^2 C^2\cos\theta_s^2}{j\,2\pi f\,\gamma'_G}\left(1 - \frac{2a}{l_b}\frac{e^{l_b/2a}-e^{-l_b/2a}}{e^{l_b/2\beta a}+e^{-l_b/2\beta a}}\right)E_X , \tag{23}$$

$1/a$ being the square root of the complex number $1/a^2 = j\,2\pi f\,\gamma'_G/K_{22}$.

In the TGB_A phase

$$\langle P_{X_s}\rangle = \frac{\epsilon_0^2\chi^2 C^2}{\alpha(T-T_C)+j2\pi f\gamma_s} \times\left(1 - \frac{2a}{l_b}\frac{e^{l_b/2a}-e^{-l_b/2a}}{e^{l_b/2\beta a}+e^{-l_b/2\beta a}}\right)E_X , \tag{24}$$

$1/a$ being the square root of the complex number $1/a^2 = [\alpha(T-T_C)+j2\pi f\gamma_s]/K_{22}$. Once again, these kinds of

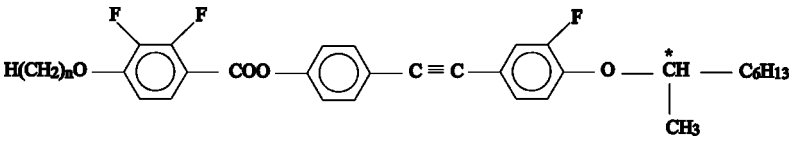

FIG. 4. Chemical formula of the chiral tolane series $n\mathrm{F}_2BT\mathrm{FO}_1M_7$.

formulas containing hyperbolic functions of complex numbers are not convenient, so we prefer the next approximate expressions of the dielectric strengths.

For the Goldstone mode of the TGB_C phase

$$\hat{\epsilon}_G(f) \simeq \frac{\epsilon_0(\chi C)^2}{H_2} \frac{\cos^2\theta_S}{1+j\dfrac{f}{f_G}}, \tag{25}$$

where f_G is the relaxation frequency

$$f_G = \frac{H_2}{2\pi\gamma_G'},$$

and for the soft mode of the TGB_A phase

$$\hat{\epsilon}_s(f) \simeq \frac{\epsilon_0(\chi C)^2}{\alpha(T-T_C)+H_2} \frac{1}{1+j\dfrac{f}{f_S}}, \tag{26}$$

where the relaxation frequency is

$$f_S = \frac{\alpha(T-T_C)+H_2}{2\pi\gamma_S}.$$

We point out that the approximations leading, respectively, from Eqs. (18), (23), and (24) to (19), (25), and (26) are not immediate. We have verified their validity with the help of numerical calculations in the TGB_C phase for $0.5 < \beta < 1$ whatever l_b is, and in the TGB_A phase for $0.25 < \beta < 1$ and l_b such that $0 < H_2/\alpha(T-T_C) < \infty$ (we anticipate here the experimental results).

The main advantages of Eqs. (25) and (26) are first, the definition of a single relaxation frequency instead of a weak distribution, second, the clear separation of the thermic $\alpha(T-T_C)$ and elastic (H_2) contributions, and third, the simplicity of the elastic term H_2 expressed with the anchoring parameter β and the block width l_b.

III. EXPERIMENT

Four compounds of the chemical series $n\mathrm{F}_2BT\mathrm{FO}_1M_7$, synthesized by Nguyen [3], are studied. Figure 4 depicts its chemical formula. The exhibited phases sequences of the studied terms ($n=9$ to 12) are summarized in Table I.

The dielectric measurement technique is described elsewhere [17]. The planar orientation of the samples is achieved with a polyvinyl alcohol coating and rubbing. In order to compare experimental results obtained on different compounds, all studied samples have roughly the same thickness ($\simeq 25$ μm), which is larger than the helical pitch. To achieve a good alignment, the cells are filled by capillarity in the isotropic phase and cooled slowly to the N^* phase. The orientation is controlled by using a polarizing microscope during the experiments. The applied electric field is perpendicular to the Sm-C^* helical axis and parallel to the TGB_C, TGB_A, and N^* axis. The measurements are analyzed using the Cole-Cole formula corresponding to m distributed relaxation process and a static conductivity σ,

$$\epsilon^\star = \epsilon_\infty + \sum_{i=1}^{m} \frac{\Delta\epsilon_i}{1+(j\,f/f_{ci})^{1-\alpha_i}} + \frac{\sigma}{j\,2\pi f\epsilon_0},$$

where ϵ_∞ is the high-frequency limit of the dielectric permittivity, α_i is the distribution parameter, f_{ci} is the critical or the relaxation frequency, and $\Delta\epsilon_i$ is the dielectric strength. The temperature dependencies of different dielectric processes are reported and discussed.

IV. DIELECTRIC MEASUREMENTS RESULTS AND DISCUSSION

A. Compound $n=9$

In addition to the Sm-C^* and N^* phases, this compound presents two smectic-A-like phases, namely Sm-A and TGB_A (see Table I). At high temperature and far from the smectic-A–smectic-C phase transition, the dielectric amplitudes are small and the relaxation frequencies high, particularly in the N^* phase. Furthermore, the ITO artifact masks the relaxation modes at high frequencies [15] and therefore it is difficult to extract the accurate values of the dielectric strength and critical frequencies from the dielectric spectra [18]. For these reasons, we do not give any experimental result in the N^* phase of this compound. Figures 5 and 7 show, respectively, the dielectric amplitude $\Delta\epsilon$ and the relaxation frequency f_c

TABLE I. Phase sequences of compounds $n=9$–12 of the $n\mathrm{F}_2BT\mathrm{FO}_1M_7$. •, phase exists; -, phase does not exist.

n	K	Sm-C^*	Sm-A	TGB_C	TGB_A	N^*	BP	I
9	•	•	•	-	•	•	•	•
10	•	•	-	-	•	•	•	•
11	•	•	-	•	•	•	•	•
12	•	•	-	•	-	•	•	•

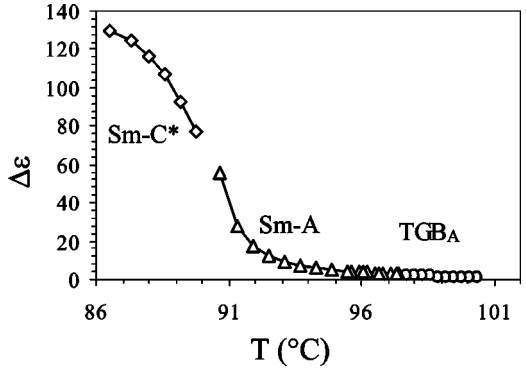

FIG. 5. Dielectric amplitude ($\Delta\epsilon$) versus temperature for the $9F_2BTFO_1M_7$ compound.

variations versus temperature obtained in TGB_A, Sm-*A*, and Sm-*C** phases in cooling. In the TGB_A phase, $\Delta\epsilon$ increases from 0.95 at 100.4 °C to 2.7 at 97.4 °C and f_c decreases from 225 kHz to ≃77.4 kHz. In the Sm-*A* phase, $\Delta\epsilon$ increases from 2.7 to about 56 at the Sm-*A*–Sm-*C** transition temperature, which occurs at 90.3 °C, and the f_c decreases to reach 3 kHz. In the Sm-*C** phase, the Goldstone mode amplitude increases to approximately 130 and the critical frequency decreases to reach a value lower than 1 kHz far from the Sm-*A*–Sm-*C** transition temperature.

In the Sm-*A* phase, the inverse of the dielectric strength $\Delta\epsilon^{-1}(T)$ and the relaxation frequency $f_c(T)$ (see Figs. 6 and 7) are linearly dependent on the temperature $(T\text{-}T_C)$ in accordance with the following formulas:

$$\Delta\epsilon^{-1}(T)\approx\frac{\alpha}{\epsilon_0\chi^2C^2}(T-T_C)$$

and

$$f_c(T)\approx\frac{\alpha}{2\pi\gamma_S}(T-T_C).$$

The TGB_A–Sm-*A* phase transition occurs at 97.4 °C. This transition is well identified by the slope changes of $\Delta\epsilon^{-1}(T)$ and $f_c(T)$. In the TGB_A phase, the difference between the experimental values and the values extrapolated from the

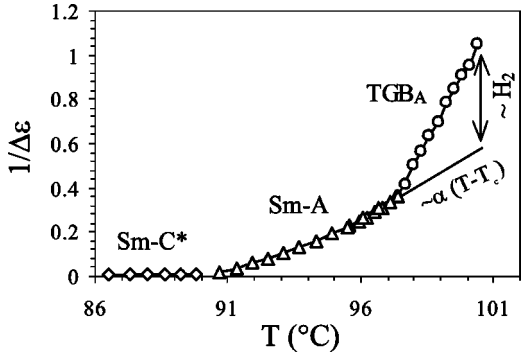

FIG. 6. Points and lines: $\Delta\epsilon^{-1}$ versus temperature for the $9F_2BTFO_1M_7$ compound. Line: extrapolation of $\Delta\epsilon^{-1}$ of the Sm-*A* phase to the TGB_A phase existence domain.

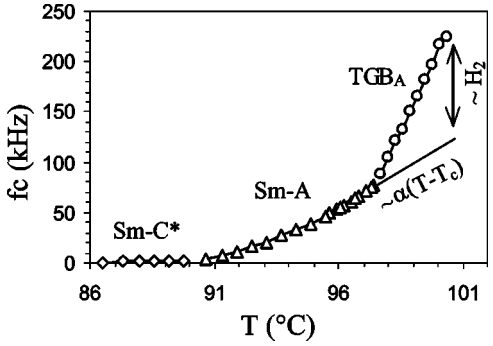

FIG. 7. Points and lines: critical frequency versus temperature for the $9F_2BTFO_1M_7$ compound. Line: extrapolation of the relaxation frequency of the Sm-*A* phase to the TGB_A phase existence domain.

Sm-*A* phase directly highlight the existence of the H_2 elastic parameter (see Figs. 6 and 7). The contribution of this parameter to the inverse of the dielectric strength is added in the TGB_A to the $\alpha(T-T_C)$ one. The H_2 contribution starts at the Sm-*A* –TGB_A phase transition with a zero value and increases with the temperature in the TGB_A phase; this behavior is easily understandable via the variation of the TGB block width l_b; likewise the helical pitch, l_b, diverges at the TGB_A–Sm-*A* transition and decreases at higher temperatures [7,8]; a quantitative analysis will be done in Sec. V B.

The variations of H_2 also follow a linear law according to the temperature. Table II summarizes the calculated slopes of the inverse of the dielectric strength and the critical frequency on both sides of the TGB_A–Sm-*A* phase transition.

We can note from Table II that $\Delta\epsilon^{-1}(T)$ and $f_c(T)$ variations versus temperature are more than three times larger in the TGB_A than in the Sm-*A* phase. In addition, since in the Sm-*A* phase

$$\left(\frac{d\,\Delta\epsilon^{-1}}{d\,T}\right)_{\text{Sm-}A}=\frac{\alpha}{\epsilon_0\chi^2C^2},$$

$$\left(\frac{d\,f_c}{d\,T}\right)_{\text{Sm-}A}=\frac{\alpha}{2\pi\gamma_S}, \tag{27}$$

and in the TGB_A phase

$$\left(\frac{d\,\Delta\epsilon^{-1}}{d\,T}\right)_{TGB_A}=\frac{\alpha}{\epsilon_0\chi^2C^2}+\frac{1}{\epsilon_0\chi^2C^2}\frac{d\,H_2}{d\,T},$$

TABLE II. $\Delta\epsilon^{-1}(T)$ and $f_c(T)$ slopes on both sides of the TGB_A–Sm-*A* transition of the $9F_2BTFO_1M_7$ compound.

	$d\Delta\epsilon^{-1}/dT(°C^{-1})$	$df_c/dT(\text{kHz}\,°C^{-1})$
TGB_A	0.23	50.5
Sm-*A*	0.07	14.3
Ratio TGB_A/Sm-*A*	3.3	3.5

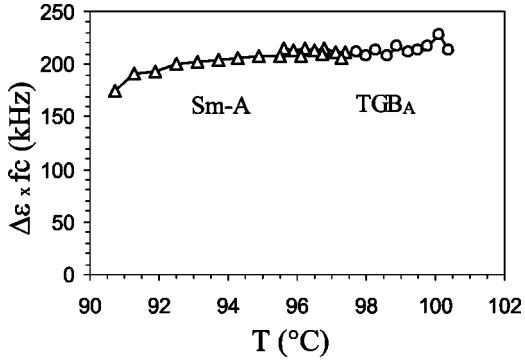

FIG. 8. $\Delta\epsilon\times f_c$ versus temperature on both sides of the TGB_A–Sm-A transition of the $9F_2BTFO_1M_7$ compound.

$$\left(\frac{d\,f_c}{d\,T}\right)_{TGB_A}=\frac{\alpha}{2\pi\gamma_S}+\frac{1}{2\pi\gamma_S}\frac{d\,H_2}{d\,T}, \tag{28}$$

it appears that $dH_2/dT\simeq 2\alpha$. This result supposes that the coefficient $\epsilon_0\chi^2C^2$ and the viscosity γ_S are constant in each phase and do not vary from one phase to the other one. This assumption is confirmed by the following two facts.

(a) The ratios $(d\,\Delta\epsilon^{-1}/d\,T)_{TGB_A}/(d\,\Delta\epsilon^{-1}/d\,T)_{Sm\text{-}A}$ and $(d\,f_c/d\,T)_{TGB_A}/(d\,f_c/d\,T)_{Sm\text{-}A}$ have approximately the same value.

(b) The product of the experimental dielectric strength and the relaxation frequency ($\Delta\epsilon\times f_c=(\epsilon_0\chi^2C^2/2\pi\gamma_s)$ in theory) remains roughly equal and practically constant ($\simeq$200 kHz, see Fig. 8) on both sides of the TGB_A–Sm-A phase transition.

In conclusion, our study highlights the existence of an elastic parameter H_2 in the TGB_A phase whose contribution to the dielectric behavior is added to the thermal coefficient $\alpha(T-T_C)$ characteristic of the Sm-A phase. The elastic parameter H_2 is equal to zero at the TGB_A–Sm-A transition and has the same magnitude as $\alpha(T-T_C)$ a few degrees higher. Therefore, in comparison with the Sm-A phase, the soft mode amplitudes are weaker and the relaxation frequencies higher in the TGB_A phase.

B. Compound $n=10$

Contrary to the previous compound, this one does not exhibit the Sm-A phase. Its phases sequence is

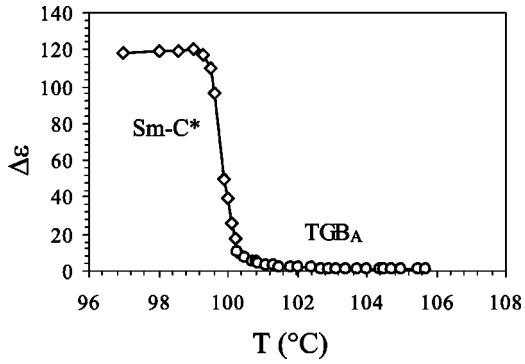

FIG. 9. Dielectric amplitude versus temperature for the $10F_2BTFO_1M_7$ compound.

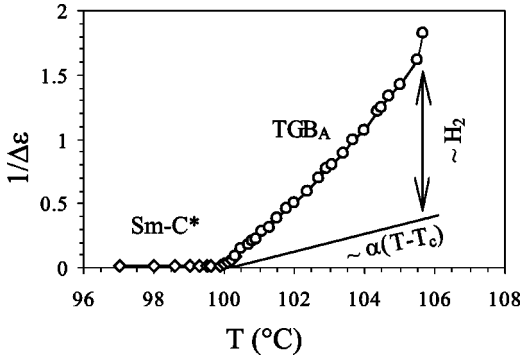

FIG. 10. Points and lines: $\Delta\epsilon^{-1}$ versus temperature for the $10F_2BTFO_1M_7$ compound. Line: $\Delta\epsilon^{-1}$ for the Sm-A phase of the $9F_2BTFO_1M_7$ compound.

Sm-C*, TBG_A, N*. In the N* phase, the dielectric amplitudes are very small and the relaxation frequencies are high; so, for the same reasons as announced in Sec. IV A, measurements of the dielectric spectra become accurate only for temperatures lower than 105.7 °C. Experimental results obtained on cooling, in the temperature range of 97 °C–105.7 °C, are drawn in Figs. 9–11. At 105.7 °C, the dielectric amplitude $\Delta\epsilon=0.6$ and overtakes 10.5 at 100.3 °C while the relaxation frequency f_c decreases from 290 kHz to about 15 kHz. The TGB_A–Sm-C* phase transition happens between $T=100.2$ °C and 100 °C where $\Delta\epsilon$ is roughly equal to 40.

We can notice that in the TGB_A phase, $\Delta\epsilon$ is small and f_c high compared to the obtained values in the Sm-A phase of the compound $n=9$: experimental values of $\Delta\epsilon^{-1}$ and f_c are about four times higher in the TGB_A phase of the compound $n=10$ compared to the Sm-A phase of $n=9$. Figures 10 and 11 clearly show that H_2 starts from zero at the Sm-C*–TGB_A transition and increases in the TGB_A phase. We can again understand this behavior via l_b variations: l_b diverges at the TGB_A–Sm-C* transition and decreases at higher temperatures [4,8]; the quantitative analysis will be given in Sec. V A.

As for the $n=9$ compound, the inverse of the dielectric strength $\Delta\epsilon^{-1}(T)$ and the relaxation frequency $f_c(T)$ are linearly dependent on the temperature in the TGB_A phase.

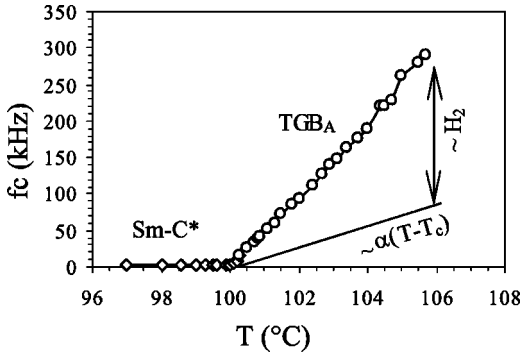

FIG. 11. Points and lines: critical frequency versus temperature for the $10F_2BTFO_1M_7$ compound. Line: critical frequency for the Sm-A phase of the $9F_2BTFO_1M_7$ compound.

TABLE III. $\Delta\epsilon^{-1}(T)$ and $f_c(T)$ slopes in the TGB_A phase of the $10F_2BTFO_1M_7$ compound.

	$d\,\Delta\epsilon^{-1}/d\,T(°C^{-1})$	$d\,f_c/d\,T(\text{kHz}\,°C^{-1})$
TGB_A	0.29	54.3

Calculated slopes of these curves are gathered in Table III.

Tables II and III show that $\Delta\epsilon^{-1}(T)$ and $f_c(T)$ slopes are, on one hand, of the same order of magnitude in the TGB_A phases of the compounds $n=9$ and $n=10$ and, on the other hand, four times higher than in the Sm-*A* phase of the compound $n=9$. The difference between the TGB_A and the Sm-*A* phases can again be explained by the elastic parameter H_2 contribution: H_2 is approximately three times larger than $\alpha(T-T_C)$ and $d\,H_2/d\,T\simeq 3\alpha$.

In the Sm-*C** phase, the Goldstone mode is well resolved: the dielectric strength increases swiftly from 40 at 100 °C to reach 118 at 99.3 °C and remains practically constant for lower temperatures; the relaxation frequency f_c is then approximately equal to 1.5 kHz. This increase of the dielectric amplitude is probably due to the helical pitch ($p_{\text{Sm-}C*}$) variations according to temperature. Indeed, the Sm-*C** phase Goldstone mode strength is given by the following formula [19]:

$$(\Delta\epsilon_G)_{\text{Sm-}C*}=\frac{1}{2}\frac{\epsilon_0\chi^2C^2}{K_{33}q^2_{\text{Sm-}C*}}, \tag{29}$$

where K_{33} is the bend elastic constant and $q_{\text{Sm-}C*}=(2\pi/p_{\text{Sm-}C*})$ $(\Delta\epsilon_G)_{\text{Sm-}C*}$ is therefore closely related to the helical pitch of the Sm-*C** phase. Close to the Sm-*C**–TGB_A transition, the helical pitch swiftly varies from about 1 μm (below 99 °C) to 0.6 μm (at 100 °C) [4] (this anomaly of $p_{\text{Sm-}C*}$ is very common), so the swift decrease of $\Delta\epsilon$, $\Delta\epsilon(100)/\Delta\epsilon(99.3)\simeq 1/2.95$ can be completely understood by the decreases of $p_{\text{Sm-}C*}$, $p^2(100)/p^2(99.3)\simeq 1/2.8$. Moreover, this analysis seems to indicate that once again $\epsilon_0\chi^2C^2$ is quasi-temperature-independent.

To study the behavior of the viscosities in the Sm-*C** and TGB_A phases, we consider the product $\Delta\epsilon\times f_c$, which is given by the following formula:

$$(\Delta\epsilon\times f_c)_{\text{Sm-}C*}=\frac{1}{2}\frac{\epsilon_0\chi^2C^2}{2\pi\gamma_G},$$

$$(\Delta\epsilon\times f_c)_{TGB_A}=\frac{\epsilon_0\chi^2C^2}{2\pi\gamma_s}. \tag{30}$$

Figure 12 shows the experimental values of $\Delta\epsilon\times f_c$ variations according to temperature. One can see three distinct areas on this curve. In the Sm-*C** phase, far from the transition temperature, this product is practically constant and equal to 180 kHz. It starts to decrease in the Sm-*C** phase at approximately 1.5 °C from the transition temperature to

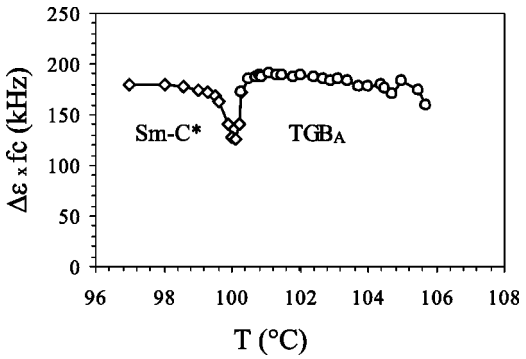

FIG. 12. $\Delta\epsilon\times f_c$ versus temperature on both sides of the TGB_A–Sm-*C** transition of the $10F_2BTFO_1M_7$ compound.

reach a value close to 125 kHz at the transition temperature. In the TGB_A phase, it is nearly constant and close to 190 kHz.

This last value is similar to values found in TGB_A and Sm-*A* phases of $n=9$. The two compounds have then similar soft mode viscosities γ_S through these phases (TGB_A for $n=10$, Sm-*A* and TGB_A for $n=9$). On the other hand, in the Sm-*C** phase of $n=9$ at temperatures lower than 98.5 °C, the Goldstone mode viscosity γ_G appears to be quasiconstant, with a value close to the half value of γ_S [we point out the presence in Eq. (30) of a coefficient $\frac{1}{2}$ in the Sm-*C** phase and recall that $\epsilon_0\chi^2C^2$ can be supposed constant]. At higher temperature, between 98.5 °C and $T_C=100$ °C, γ_G increases by a factor of about 1.5 [$(\Delta\epsilon\times f_c)$ decreases]. The behavior of $(\Delta\epsilon\times f_c)$ in the Sm-*C** temperature domain $[T_C-1.5\,°C,\ T_C]$ seems to reveal an anomaly of the rotational viscosity γ_G near the transition temperature, this anomaly could be connected to the amplitudes of the molecular motions that are large at low temperature and become weaker close to the transition temperature T_C.

C. Compound $n=11$

The phases sequence of this compound is Sm-*C**, TGB_C, TGB_A, *N**, it presents successively two TGB phases. Experimental results are drawn in Figs. 13–15. Similarly to the previous compound, experimental spectra

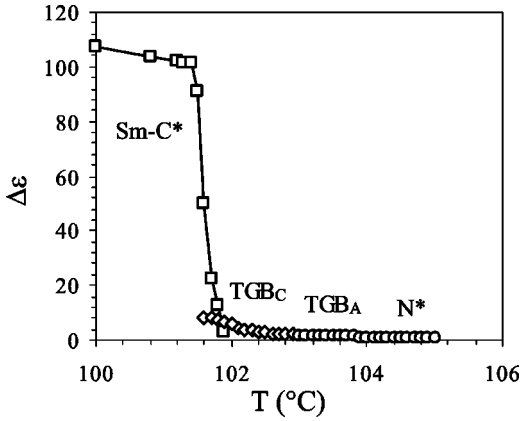

FIG. 13. Dielectric amplitude versus temperature for the $11F_2BTFO_1M_7$ compound.

become exploitable in the lower limit of the existence domain of the N^* phase at 105 °C. At this temperature, the dielectric strength $\Delta\epsilon_{N^*}$ is $\simeq 0.6$ and the relaxation frequency $(f_c)_{N^*}$ is $\simeq 150$ kHz. The N^*-TGB_A phase transition happens at 104.5 °C. In the TGB_A phase, the dielectric strength increases gently when decreasing temperature, to reach $(\Delta\epsilon)_{TGB_A} \simeq 1.8$ at the lower limit of the existence domain of this phase, the frequency of relaxation $(f_c)_{TGB_A}$ is $\simeq 60.5$ kHz. The TGB_C-TGB_A phase transition occurs at 102.9 °C. One can note that in spite of the change of the dielectric mode (soft mode in the TGB_A phase and a Goldstone mode in the TGB_C phase), the dielectric amplitudes remain low and the experimental curves are continuous at the TGB_A-TGB_C phase transition. The dielectric strength increases from 2 at 102.8 °C to 6.1 at 102 °C and the relaxation frequency decreases from 58.4 kHz to 22.6 kHz.

The TGB_C–Sm-C^* transition starts at 101.9 °C and persists 0.5 °C below this temperature. In this biphasic domain, two dielectric modes, which correspond to the Goldstone modes of the TGB_C and Sm-C^* phases, are detected; the dielectric strength (Fig. 13) increases rapidly with the Sm-C^* proportion to reach a value close to 105 right in the Sm-C^* phase at 101.4 °C, the critical frequency is then equal to 1.3 kHz.

Except in the immediate vicinity of the transition temperatures, the inverse of the dielectric strength and the relaxation frequencies are linearly dependent on the temperature in the N^*, TGB_A, and TGB_C phases. The transition from one phase to another appears by changes of the slopes (see Figs. 14 and 15). The TGB_A-TGB_C phase transition is more clearly visible on the relaxation frequency curve in which appears a very visible anomaly. The calculated slopes in the TGB_A and TGB_C phases are gathered in Table IV. We can see that these slopes differ approximately from 10% to 15% in the TGB_A and TGB_C phases. This difference can be assigned to the nature of the relaxation mode (soft mode in the TGB_A phase and Goldstone mode in the TGB_C phase).

Unlike the H_2 of compounds $n=9$ and 10, which start from zero, H_2 of compound $n=11$ is large from the beginning of the TGB_A phase (Figs. 14 and 15); this behavior is related to the finite value of the block width l_b at the

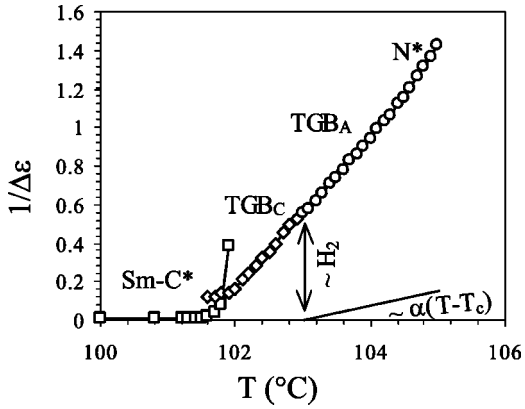

FIG. 14. Points and lines: $\Delta\epsilon^{-1}$ versus temperature for the $11F_2BTFO_1M_7$ compound. Line: $\Delta\epsilon^{-1}$ for the Sm-A phase of the $9F_2BTFO_1M_7$ compound.

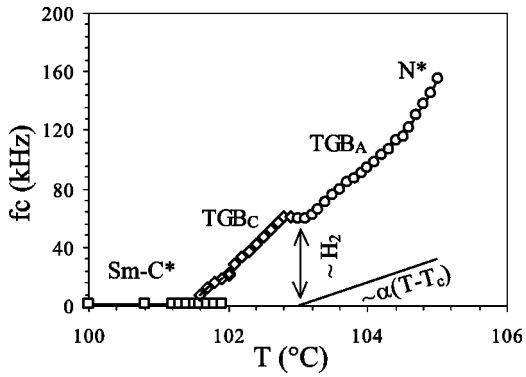

FIG. 15. Points and lines: Critical frequency versus temperature for the $11F_2BTFO_1M_7$ compound. Line: relaxation frequency for the Sm-A phase of the $9F_2BTFO_1M_7$ compound.

TGB_C-TGB_A phase transition. Indeed, for this compound l_b diverges only for a lower temperature, close to the TGB_C–Sm-C^* phase transition. When the temperature increases, l_b decreases and H_2 increases linearly. The slope $dH_2/dT \simeq 6\alpha$ is large compared to the values obtained for the previous compounds (approximately 2α for $n=9$ and 3α for $n=10$). In summary, in the TGB_A, the soft mode strength is very small and the relaxation frequencies very high compared to those of the classical Sm-A phase.

In the TGB_C phase, the Goldstone mode dielectric strength is small compared to the Sm-C^* phase, this means that $(H_2)_{TGB_C} \gg K_{33} q^2_{\text{Sm-}C^*}$ [Eqs. (25) and (29)]: the Goldstone mode strength drops by a factor higher than 16 in the TGB_C phase compared to that of the Sm-C^* one. H_2 will be quantitatively studied in Sec. V for the TGB_A and TGB_C phases.

The transformation of the TGB_A soft mode into the TGB_C Goldstone one seems to be continuous. This behavior is in agreement with our theoretical predictions [see Eqs. (13) and (19)]. In the TGB_A phase, the thermal term, $\alpha(T-T_C)$, contribution to the dielectric relaxation becomes weak close to transition temperature, this term vanishes at the TGB_A-TGB_C phase transition temperature; in the TGB_C phase, the dielectric strength is then only governed by the parameter H_2. The dielectric strength continuity at the transition between the TGB_A and the TGB_C phases seems then to show that the $\epsilon_0\chi^2C^2$ term is continuous at this transition. On the other hand, the behavior of the experimental relaxation frequency according to temperature seems to point out an anomaly [20,21] of the rotational viscosity.

In order to estimate the viscosity, we study now the product $\Delta\epsilon \times f_c$. The theoretical expressions are

TABLE IV. $\Delta\epsilon^{-1}(T)$ and $f_c(T)$ slopes on both sides of the TGB_C-TGB_A transition of the $11F_2BTFO_1M_7$ compound.

	$d\Delta\epsilon^{-1}/dT$(°C^{-1})	df_c/dT(kHz °C^{-1})
TGB_A	0.48	41.3
TGB_C	0.43	49.8
Ratio TGB_A/TGB_C	1.1	0.8

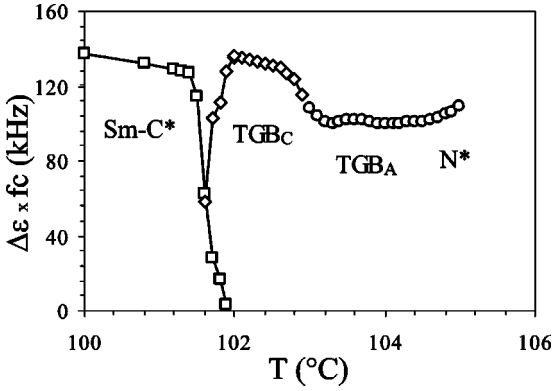

FIG. 16. $\Delta\epsilon\times f_c$ versus temperature on both sides of the TGB_C–Sm-C^* and TGB_C-TGB_A transitions of the $11F_2BTFO_1M_7$ compound.

$$(\Delta\epsilon\times f_c)_{\text{Sm-}C^*}=\frac{1}{2}\frac{\epsilon_0\chi^2C^2}{2\pi\gamma_G},$$

$$(\Delta\epsilon\times f_c)_{\text{TGB}_A}=\frac{\epsilon_0\chi^2C^2}{2\pi\gamma_s}, \tag{31}$$

$$(\Delta\epsilon\times f_c)_{\text{TGB}_C}=\frac{\epsilon_0\chi^2C^2}{2\pi\gamma_G'}\cos^2\theta_s,$$

where γ_S is the TGB_A phase soft mode viscosity, γ_G and γ_G' are, respectively, the Goldstone mode viscosities of the Sm-C^* and the TGB_C phases. Note that the term $\cos^2\theta_s$ is close to unity [22].

The experimental values of $\Delta\epsilon\times f_c$ are plotted in Fig. 16. Except near the transition temperatures this product is practically constant: about 130 kHz in the TGB_C and Sm-C^* phases and slightly lower in the TGB_A phase ($\simeq$100 kHz). This mean that the viscosities γ_S in the TGB_A phase and γ_G' in the TGB_C phase are quasiconstant. The soft mode viscosity γ_S is slightly higher than the TGB_C Goldstone mode viscosity γ_G', $\gamma_s\simeq1.3\gamma_G'$. Moreover, the equality of $\Delta\epsilon\times f_c$ in the Sm-C^* and TGB_C phases means that the TGB_C Goldstone mode viscosity γ_G' is twice higher than the Sm-C^* viscosity γ_G: $2\gamma_G\simeq\gamma_G'$ [see Eq. (31)]. This result seems to be abnormal since both modes concern molecular rotations on the smectic cones. These modes differ, however, by their dielectric amplitudes, which are much larger in the Sm-C^* phase than in the TGB_C; the molecular movements are thus much larger in the Sm-C^* than in the TGB_C phase; the decrease of the viscosity at the TGB_C–Sm-C^* phase transition can therefore be interpreted as a consequence of the magnitude of these molecular movements.

In brief, the viscosity appears to be closely related to the magnitude of the molecular movements: the amplitudes are as high as the viscosity is small. The magnitude of the molecular movements seems to be more predominant in the TGB phases than the dielectric mode type.

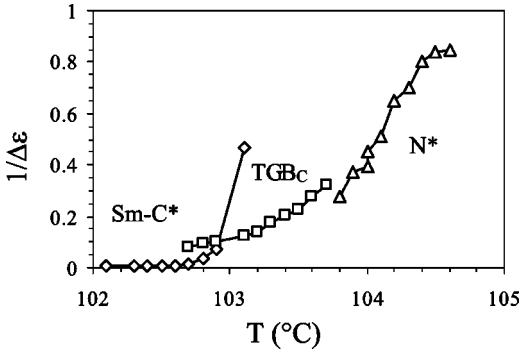

FIG. 18. $\Delta\epsilon^{-1}$ versus temperature for the $12F_2BTFO_1M_7$ compound.

D. Compound $n=12$

The phases sequence of this compound is Sm-C^*, TGB_C, N^*. Compared to the previous compound, this one does not present the TGB_A phase (see Table I). Experimental results obtained on cooling are given in the three phases.

The dielectric strength, its inverse and the critical frequency are given in Figs. 17–19. In the N^* phase, the dielectric strength of the soft mode $(\Delta\epsilon)_{N^*}$ is small but approximately two times greater than for the $n=11$ compound. It ranges between 1 and 1.5 when the temperature varies from 104.8 °C to 104.2 °C. The relaxation frequency $(f_c)_{N^*}$ decreases from roughly 100 kHz to 60.7 kHz for the same temperature interval. The N^*-TGB_C phase transition occurs

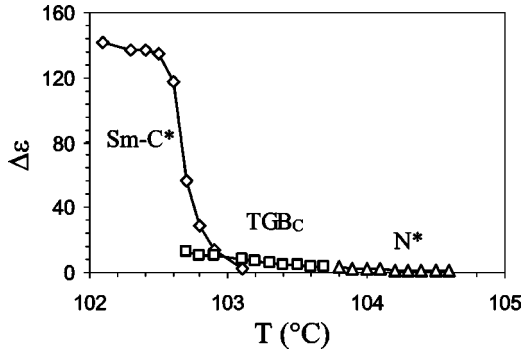

FIG. 17. Dielectric amplitude versus temperature for the $12F_2BTFO_1M_7$ compound.

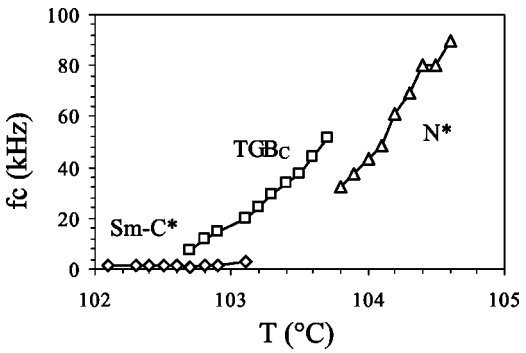

FIG. 19. Critical frequency versus temperature for the $12F_2BTFO_1M_7$ compound.

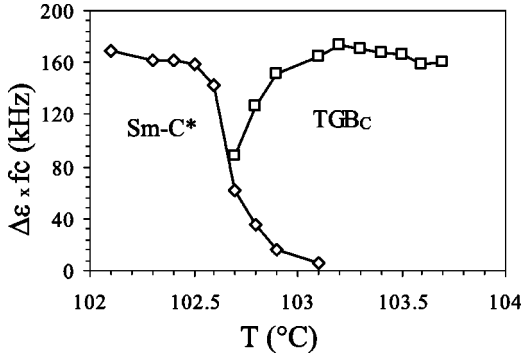

FIG. 20. $\Delta\epsilon\times f_c$ versus temperature on both sides of the TGB_C–Sm-C^* transition of the $12F_2BTFO_1M_7$ compound.

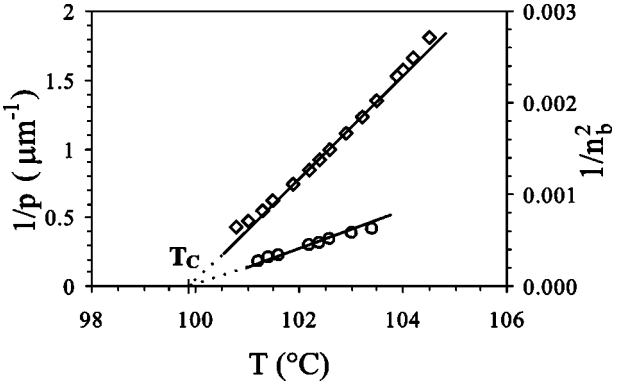

FIG. 21. ($\diamond$), $1/p$ and ($\bigcirc$), $1/n_b^2$ in the TGB_A phase of $10F_2BTFO_1M_7$ compound.

at 104.1 °C and spreads over 0.5 °C. The N^* phase disappears completely at 103.6 °C. The existence temperature domain of the TGB_C phase is 0.5 °C. In the biphasic domain of the N^* and TGB_C phases ($103.6\,°C \leqslant T \leqslant 104.1\,°C$), measured spectra correspond to the contribution of two modes, namely, the soft mode of the N^* phase, which is dominant in the temperature range of 103.8 °C to 104.1 °C, and the Goldstone mode of the TGB_C phase. The distribution of the experimental spectra does not allow to separate the two contributions. The TGB_C–Sm-C^* phase transition starts to happen at 103.1 °C, the TGB_C phase vanishes at 102.6 °C. At the vicinity of the TGB_C–Sm-C^* phase transition, two relaxation modes are detected. They are the two well-resolved Goldstone modes of the TGB_C and Sm-C^* phases. As for the previous compound and when the temperature decreases, the dielectric strength $\Delta\epsilon$ increases abruptly after passing through the TGB_C phase to reach 140 in the Sm-C^* phase. Once again, we can note that the Goldstone mode dielectric amplitudes are much smaller in the TGB_C than in the Sm-C^* phase. The critical frequency is approximately equal to 1.2 kHz in the whole Sm-C^* phase.

On both sides of the N^*-TGB_C transition, the slopes of the inverse of the dielectric strength are respectively, close to $0.60\,°C^{-1}$ in the N^* phase and to $0.32\,°C^{-1}$ in the TGB_C phase (Fig. 18).

Like for the previous compounds, we study now the product $\Delta\epsilon\times f_c$ in order to give an account of the viscosity variations according to temperature. Figure 20 shows that in the TGB_C and Sm-C^* phases, the product $\Delta\epsilon\times f_c$ is approximately constant, this means that the viscosities are also quasiconstant in these phases. Considering Eqs. (31), it appears that the rotational viscosity γ_G in the Sm-C^* phase is twice as small as the viscosity γ_G' of the TGB_C phase though both concern rotations on the cone. Once again, it seems that the greater the molecular movements are, smaller the rotational viscosity is.

V. ANCHORING STRENGTH AND DISCUSSION

We have seen above that the dielectric collective modes in the TGB_A and TGB_C phases are reduced in comparison with those of the classical smectic phases Sm-A and Sm-C^*. This behavior is due to the elastic parameter H_2, which is related to the blocks size and the anchoring strength coefficient β at the grain boundaries [see Eqs. (14) and (20)]. Next we will calculate, in the TGB phases, the anchoring strength and its variations according to temperature for all studied compounds.

A. $n=10$

In the TGB_A phase, the anchoring strength β can be calculated by inversion of equation (19) using the dielectric strength results,

$$\frac{\beta^2}{1-\beta^2/3}=\frac{\epsilon_0\chi^2C^2}{8K_{22}}l_b^2\left[\Delta\epsilon^{-1}-\frac{\alpha}{\epsilon_0\chi^2C^2}(T-T_C)\right]. \quad (32)$$

Three coefficients must be predetermined. The first one can be deduced from the expression of the dielectric strength of the Goldstone mode in the Sm-C^* phase [see Eq. (29)]: the quantity

$$F=\frac{\epsilon_0\chi^2C^2}{8K_{22}}=\pi^2\frac{K_{33}}{K_{22}}\left(\frac{\Delta\epsilon}{p^2}\right)_{\text{Sm-}C^*}\simeq\pi^2\left(\frac{\Delta\epsilon}{p^2}\right)_{\text{Sm-}C^*},$$

calculated from the pitch values and dielectric results in the Sm-C^* phase, is found to be equal to 1285.

A second coefficient, $\alpha/\epsilon_0\chi^2C^2$, is the slope of $\Delta\epsilon^{-1}$ according to $(T-T_C)$ in the Sm-A phase. This quantity is not available for $n=10$ because this compound does not possess the Sm-A phase. For this reason, we use the values 0.07 obtained for the $n=9$ (see Table II) and also for mixtures of $n=9$ and 10 compounds (not reported here).

To calculate the last parameter l_b^2 we use pitch values measured by ourselves [4] and the values of the number of blocks per pitch n_b measured by x-ray diffraction by Navailles *et al.* [8]. The results, given in the Fig. 21, clearly show that both $1/p$ and $1/n_b^2$ have linear variations with temperature, so l_b appears to vary like the square root of the helical pitch, $l_b=A\sqrt{p}$. Note that such a relation is quite equivalent to the law $l_b\simeq l_d$ (distance between screw dislocation) first predicted by Renn and Lubensky [1] and experimentally confirmed by Navailles *et al.* [8]. We find an experimental value $A\simeq 2.25\times10^{-2}$ very close to the theoretical

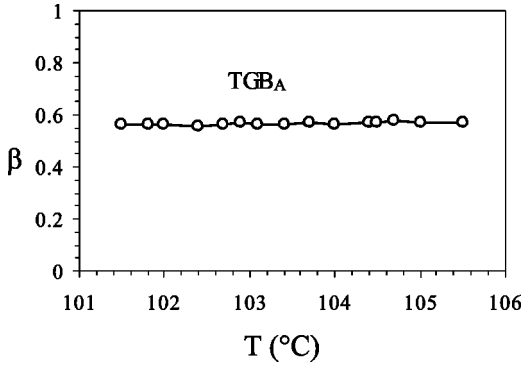

FIG. 22. Anchoring strength versus temperature for the $10F_2BTFO_1M_7$ compound.

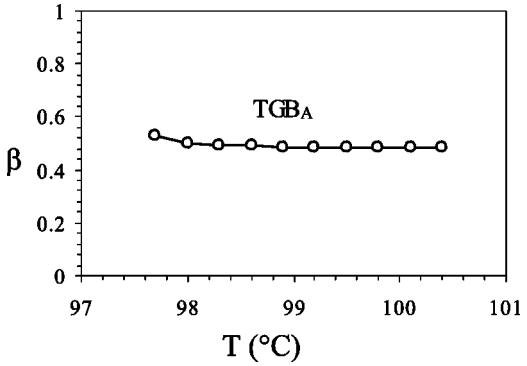

FIG. 23. Anchoring strength versus temperature for the $9F_2BTFO_1M_7$ compound.

one, $A=\sqrt{d/2\pi}\simeq 2.46\times 10^{-2}$ in which d is the layer thickness ($d\simeq 38\times 10^{-4}$ μm) [22].

The anchoring coefficient β can then be deduced from

$$\frac{\beta^2}{1-\beta^2/3}=FA^2p\left[\Delta\epsilon^{-1}-\frac{\alpha}{\epsilon_0\chi^2C^2}(T-T_C)\right]. \qquad (33)$$

As both $1/p$ (Fig. 21) and $\Delta\epsilon^{-1}$ (Fig. 10) vary linearly with temperature, β is found to be quasiconstant: Fig. 22 shows that the calculated anchoring strength β remains roughly equal to 0.56 in the whole temperature range of the TGB_A phase. We point out that, in order to avoid any artifact, it is essential to make a match with $T_C=99.8\,^\circ$C, the temperature for which the three quantities $1/n_b^2$, $1/p$, and $1/\Delta\epsilon$ reach zero.

B. $n=9$

The anchoring strength β at the grain boundary in the TGB_A phase of this compound is also determined from the relation (33). We use the same numerical coefficients as for the compound $n=10$; in particular, because of the unavailability of the number of blocks per pitch n_b, we adopt the same law $l_b=A\sqrt{p}$ with the same value of the coefficient $A(=2.25\times 10^{-2})$; the pitch values had been measured by ourselves [23]. A difference lies in matching the temperatures: the helical pitch diverges in the present sequence at the TGB_A–Sm-A transition temperature [23], so we have to make the temperature for which $1/p$ reduces to zero ($p\rightarrow\infty$) match the temperature of the TGB_A-Sm-A phase transition determined by dielectric measurements and for which $\Delta\epsilon^{-1}-(\alpha/\epsilon_0\chi^2C^2)(T-T_C)$ reaches zero (that is, $T=97.4\,^\circ$C). As both $1/p$ and this last quantity vary linearly with the temperature, β is again quasiconstant in the whole TGB_A phase. We find a value of β close to 0.5 (Fig. 23), which is very similar to the anchoring strength found for the previous compound $n=10$.

C. $n=11$

In the TGB_A phase of this compound, β is again determined from Eq. (33). Only the factor

$$F=\frac{\epsilon_0\chi^2C^2}{8K_{22}}=\pi^2\frac{K_{33}}{K_{22}}\left(\frac{\Delta\epsilon}{p^2}\right)_{\text{Sm-}C^*}\simeq\pi^2\left(\frac{\Delta\epsilon}{p^2}\right)_{\text{Sm-}C^*}$$

is readjusted to take into account slightly different values of $\Delta\epsilon$ and the helical pitch p in the Sm-C^* phase ($p_{\text{Sm-}C^*}=0.9$ μm, $(\Delta\epsilon)_{\text{Sm-}C^*}=100$ at $101.3\,^\circ$C, give here $F=1218$); A and $\alpha/\epsilon_0\chi^2C^2$ are supposed unchanged. We use our pitch measurement reported in [4], taking care to adjust two temperatures: the TGB_A-TGB_C transition temperature detected here ($102.9\,^\circ$C) and the transition temperature detected in the pitch measurements (the last temperature corresponds to a rapid increase of the helical pitch, which may be confused with a discontinuity [3,4]). Figure 24 shows that the anchoring coefficient β is again quasiconstant in the TGB_A phase ($\beta\simeq 0.45$) and similar to those obtained for $n=10$ and $n=9$ compounds.

In the TGB_C phase, the anchoring strength β can be calculated by using the dielectric strength expression [see Eq. (13)] rewritten as

$$\frac{\beta^2}{1-\beta^2/3}=\frac{\epsilon_0\chi^2C^2}{8K_{22}}\Delta\epsilon^{-1}l_b^2\cos\theta_S^2$$

or

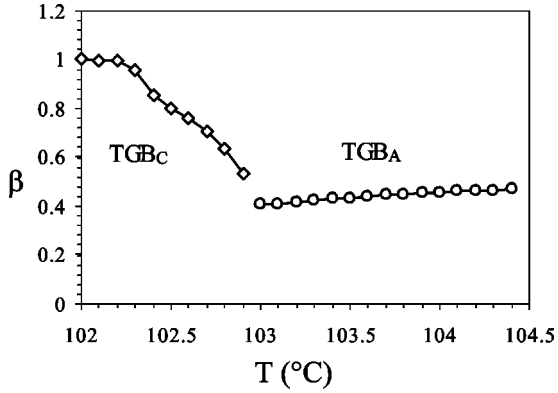

FIG. 24. Anchoring strength versus temperature for the $11F_2BTFO_1M_7$ compound.

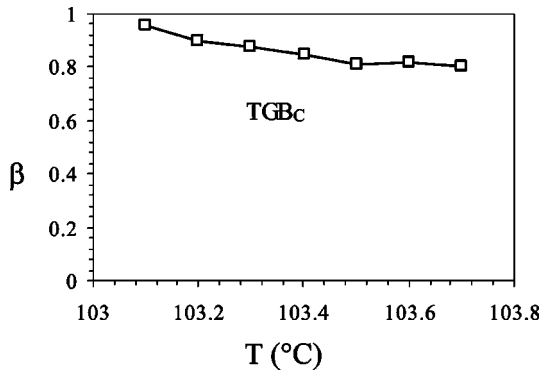

FIG. 25. Anchoring strength versus temperature for the $12F_2BTFO_1M_7$ compound.

$$\frac{\beta^2}{1-\beta^2/3} = F\Delta\epsilon^{-1}\frac{p^2}{n_b^2}\cos\theta_S^2. \tag{34}$$

We point out an important difference between TGB_C and TGB_A phases: in the TGB_A phase, n_b shows large variations according to temperature (between 60 and 40 for the compound $n=10$ [8], for example); these variations are related to those of the helical pitch by $n_b^2=p/A^2$, leading to the law $l_b^2=A^2p$; on the contrary, in the TGB_C phase, n_b remains quasiconstant [5,22,24], so $l_b^2=(1/n_b^2)p^2$ varies like the square value of the helical pitch. This difference clearly appears in formula (34) compared to Eq. (33). Figure 24 reports the anchoring coefficient β calculated with Eq. (34) using pitch values taken from [4], number of blocks per pitch $n_b\simeq 24$, and values of θ_S given by Navailles and co-workers [22,5]. β increases from approximately 0.5 at the TGB_A-TGB_C phase transition temperature (102.9 °C) to 1 at lower temperature (102 °C). A hardening of the anchoring occurs then in the TGB_C phase at temperatures going down, away from the TGB_C-TGB_A transition.

D. $n=12$

Like for the last compound, the anchoring coefficient β in the TGB_C phase of the $n=12$ compound is determined by using Eq. (34). The number n_b of the TGB blocks per pitch is equal to 18 and the tilt angle $\theta_s\simeq 18°$ [22,5]. The coefficient F is readjusted by taking into account the values of $\Delta\epsilon$ and the helical pitch in the Sm-C^* phase [$p_{\text{Sm-}C^*}\simeq 0.85$ μm and $(\Delta\epsilon)_{\text{Sm-}C^*}\simeq 140$ at 103 °C]. The helical pitch values of the TGB_C phase are taken from [4]. Figure 25, represents the anchoring strength β variations versus temperature: $\beta\simeq 1$ at low temperature (103.1 °C) and decreases slightly down to approximately 0.8 near the TGB_C-N^* transition temperature (103.7 °C). The anchoring strength β observed here is rather hard, like in the TGB_C phase of the previous compound $n=11$ at low temperature and far from the TGB_A phase.

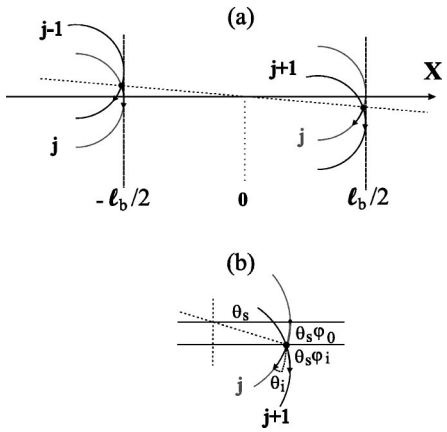

FIG. 26. Top view of the TGB_C jth block. (a) At zero field, the director is oriented according to the intersection of the two cones related to the two successive blocks. (b) Under an electric field, an induced tilt angle ensures the director continuity.

E. Discussion

In the TGB_A phase, the dielectric amplitudes are lower than in the Sm-A phase. The anchoring coefficient β is not large at the grain boundaries ($\beta\simeq 0.5$) and it is quasi-temperature-independent. The three compounds studied here are significantly different. Figures 6, 10, and 14 allow comparison of the temperature $[\alpha(T-T_C)]$ and block width $(H_2\sim 1/l_b^2)$ effects: for $n=9$, H_2 cancels out because l_b diverges at the TGB_A–Sm-A phase transition, which occurs at $T_C+7.4$ °C; for $n=10$, H_2 cancels out because l_b diverges at the Sm-C^*–TGB_A transition, i.e., at T_C exactly; for $n=11$, H_2 is great at T_C because l_b is finite (its divergence takes place at the TGB_C–Sm-C^* transition, that is, at $T_C-0.9$ °C); at a given $(T-T_C)$ value, l_b values are so very different for the three phases sequences. In other words, the three studied compounds allow to obtain $H_2/\alpha(T-T_C)$ ratios varying from 0 to ∞ (0 to $\simeq 1$ for compound $n=9$,$\simeq 3$ for $n=10$, and from $\simeq 10$ to ∞ for $n=11$). Nevertheless we observe a common anchoring property in the three cases.

In the TGB_C phase, what seems remarkable is the hardening of the anchoring when moving away from the TGB_A phase of the compound $n=11$ and the firmness of the anchoring observed in the TGB_C phase of the compound $n=12$ even at the approach of the N^* phase.

We can now ask the question of the physical origin of the anchoring coefficient β. Let us begin by the TGB_C phase. We tempt to explain its behavior with the help of the TGB_C phase description first given by Dozov [25] and backed up by optical reflectivity experimental studies [26]. In this model, the TGB_C phase is not constituted by homogeneous Sm-C^* blocks with director rotations localized in the grain boundaries; the rotation of the director is on the contrary uniformly distributed in all the block thanks to weak rotations easily realized on the smectic cone; Fig. 26(a) schematizes such a twisted structure in the absence of applied field: $\theta_S\varphi_0(X)=2\pi X/p$ for $-l_b/2<X<l_b/2$; at the grain boundary, the director is continuous and oriented along the intersection of the two smectic cones related to the two successive blocks. The electric field exerts a couple that tends to

turn the director on the first cone to the left side of the grain boundary and on the second cone to the right side of this grain boundary. If the spontaneous tilt angle of the cone is large (far from T_C for the compound $n=11$, and in the whole existence domain of the TGB_C phase for $n=12$), these two movements would break the continuity of the director and would provoke a splay deformation of very large energy density. To ensure the continuity of the director, an additional tilt is then necessary [Fig. 26(b)]; its amplitude is about $\theta_i = \varphi_{0(l_b/2)}\theta_s\varphi_i$. The associated energy density, localized near the grain boundary, is $\alpha(T_c-T)\varphi^2_{0(l_b/2)}\theta^2_s\varphi^2_i$. An additional torque, which is equal to $2\alpha(T_c-T)\varphi^2_{0(l_b/2)}\theta_s\varphi_i$, exists then near the grain boundary. The anchoring at the grain boundary can so be understood as a consequence of this torque induced by a tilt that must be added to the azimuthal rotation in order to ensure the director continuity.

On the contrary, for the TGB_A phase, the rotation of the director is probably not uniformly distributed in the whole block [because a large tilt like $\theta_0(X)=(2\pi/p)X$ would cost an energy density much larger than the energy cost of the azimuthal rotation $\theta_s\varphi_0(X)$ in the TGB_C phase]. Schematically $\theta_0(X)$ is probably close to zero in the whole block and rapidly jumps over a short distance through the grain boundary. In this area, the field induced tilt θ_i starts from $\theta_0(X)$ instead of zero; as $\theta_0(X)$ has rather large values, the electroclinic effect can become weak; the overcost energy density can be estimated using $(b/4)\theta^4$, to about $\langle \frac{3}{2} b\theta_0^2(X)\rangle\theta_i^2$. An additional torque appears then in the grain boundary, its mean value being lower than $b\theta^2_{0(l_b/2)}\theta_i$.

Briefly, the common origin of the anchoring in the two phases is the necessity to ensure the continuity of the director through the grain boundary: in the TGB_A, the induced tilt angle θ_i starts from $\theta_0(X)$ instead of zero creating a sort of saturation of the electroclinic effect in the vicinity of the grain boundary; while in the TGB_C phase, in addition to the induced rotation φ_i, an induced tilt angle θ_i, which starts from θ_s, is necessary to avoid an important splay; this tilt has a large energy cost, in particular, far from the Sm-*A*–Sm-*C* temperature transition and this may explain a larger anchoring.

Note that these considerations have to be taken only as qualitative: they do not allow us to precisely express the anchoring coefficient β according to various parameters; our analysis only allows to give a possible justification to the existence of the anchoring at the grain boundaries of the TGB phases, which appears in an obvious way in our experimental results.

Other justifications of the anchoring in the grain boundaries can be invoked: for example, the melting of the smectic order around the dislocations lines. In the TGB_A phase, the loss of smectic order reduces the coupling between the induced polarization and tilt [17,27]. In the TGB_C phase, it reduces the spontaneous polarization, diminishing the field induced azimuthal rotation (the basis of the Goldstone mode) near the dislocations. The result is the anchoring of the director by the melted regions in which the electric field is less efficient. We finally note that the last effect is also probably larger in the TGB_C phase for which the number of dislocations augments (the ratio l_b/l_d increases up to 7 [4,22]).

VI. CONCLUSION

Our theoretical and experimental studies of the dielectric properties of twist grain boundary phases TGB_A and TGB_C show that in the planar orientation, these phases are, respectively, subject to the soft and Goldstone modes. Nevertheless, these modes obey in these phases laws that noticeably differ from the Sm-*A* and Sm-*C** phase.

In the Sm-*A* phase, the main parameter that governs the soft mode is the distance to the Sm-*A*–Sm-*C* transition [through the quantity $\alpha(T-T_C)$]. In the Sm-*C** phase, the parameter that governs the Goldstone mode is related to the field induced distortion of the helical structure (though $K_{33}q^2$). In the TGB_A phase, appears a new elastic parameter H_2, its effect is added the thermic one, $\alpha(T-T_C)$. In the TGB_C phase, the dielectric response is totally governed by this new parameter. This elastic coefficient is due to the elastic distortion of the director, its amplitude depends strongly on the anchoring forces at the grain boundaries and on the distance between these grain boundaries.

Our experimental studies show that the amplitudes of measured modes, in TGB phases, are small in comparison with those observed in Sm-*A* and Sm-*C** phases; the action of the new elastic coefficient appears to be very efficient; it varies very much with temperature and its variations qualitatively express the block size variations. We have performed a quantitative analysis of our experimental results and have calculated an anchoring parameter; it appears that the anchoring strength is moderate in the TGB_A phase and becomes hard in the TGB_C one; this hardening seems to confirm that, contrary to the torsion of layers located at the grain boundaries, the director torsion is uniformly distributed in the blocks.

The relaxation frequencies studies reveal an anomaly of the rotational viscosity in the Sm-*C** phase close to the TGB_A phase and above all an anomaly between the Sm-*C** and TGB_C phases.

[1] S.R. Renn and T.C. Lubensky, Phys. Rev. A **38**, 2132 (1988).
[2] J. W. Goodby, M. A. Waugh, S. M. Stein, E. Chin, R. Pindak, and J. S. Patel, Nature (London) **337**, 449 (1989).
[3] H. T. Nguyen, A. Bouchta, L. Navailles, P. Barois, N. Isaert, R. J. Twieg, A. Maaroufi, and C. Destrade, J. Phys. II **2**, 1889 (1992).
[4] N. Isaert, L. Navailles, P. Barois, and H. T. Nguyen, J. Phys. II **4**, 1501 (1994).
[5] L. Navailles, P. Barois, and H. T. Nguyen, Phys. Rev. Lett. **71**, 545 (1993).

[6] L. Navailles, R. Pindak, P. Barois, and H. T. Nguyen, Phys. Rev. Lett. **74(26)**, 5224 (1995).
[7] A. Bouchta, H. T. Nguyen, L. Navailles, P. Barois, C. Destrade, F. Bougrioua, and N. Isaert, J. Mater. Chem. **5**, 2079 (1995).
[8] L. Navailles, B. Pansu, L. Gorre-Talini, and H. T. Nguyen, Phys. Rev. Lett. **81**, 4168 (1998).
[9] C. Girold, C. Legrand, N. Isaert, P. Pochat, J. P. Parneix, H. T. Nguyen, and C. Destrade, Ferroelectrics **147**, 171 (1993).
[10] H. T. Nguyen, C. Destrade, J. P. Parneix, P. Pochat, N. Isaert, and C. Girold, Ferroelectrics **147**, 181 (1993).
[11] S. Wróbel, S. Hiller, M. Pfeiffer, M. Marzec, and W. Haase, Liq. Cryst. **18**, 21 (1995).
[12] H. Xu, P. Panarin, J. K. Vij, A. J. Seed, M. Hird, and J. W. Goodby, J. Phys.: Condens. Matter **7**, 7443 (1995).
[13] F. Bougrioua, N. Isaert, C. Legrand, A. Bouchta, P. Barois, and H. T. Nguyen, Ferroelectrics **180**, 35 (1996).
[14] J. P. Parneix and C. Legrand, Ferroelectrics **84**, 199 (1988).
[15] F. Gouda, K. Skarp, and S. T. Lagerwall, Ferroelectrics **113**, 165 (1991).
[16] S. Beldon and S. J. Elston, Liq. Cryst. **26**, 143 (1999).
[17] C. Legrand, N. Isaert, J. Hmine, J. M. Buisine, J. P. Parneix, H. T. Nguyen, and C. Destrade, J. Phys. II **2**, 1545 (1992).
[18] F. Gouda, K. Skarp, G. Andersson, H. Kresse, and S. T. Lagerwall, Jpn. J. Appl. Phys., Part 1 **28**, 1887 (1989).
[19] C. Legrand and J. P. Parneix, J. Phys. (France) **51**, 787 (1990).
[20] A. Levstik, Z. Kuntjak, C. Filipič, I. Livstik, and Z. Bregar, Phys. Rev. A **42**, 2204 (1990).
[21] A. Levstik, Z. Kuntjak, C. Filipič, I. Livstik, B. Žekš, and T. Carlsson, Ferroelectrics **113**, 207 (1991).
[22] L. Navailles, Ph.D. thesis, Université of Bordeaux I, France, 1994.
[23] M. Ismaïli, A. Anakkar, G. Joly, and N. Isaert, Phys. Rev. E **61**, 519 (2000).
[24] M. H. Li, V. Laux, H. T. Nguyen, G. Sigaud, Ph. Barois, and N.I. Isaert, Liq. Cryst. **23**, 389 (1997).
[25] I. Dozov, Phys. Rev. Lett. **74**, 4245 (1995).
[26] L. Détré, G. Joly, N. Isaert, P. Barois, H. T. Nguyen, and I. Dozov, Ferroelectrics **244**, 49 (2000).
[27] Z. Li, G. A. Di Lisi, R. G. Petschek, and C. Rosenblatt, Phys. Rev. A **41**, 1997 (1990).